

# Dalton Transactions

Accepted Manuscript



This is an *Accepted Manuscript*, which has been through the Royal Society of Chemistry peer review process and has been accepted for publication.

*Accepted Manuscripts* are published online shortly after acceptance, before technical editing, formatting and proof reading. Using this free service, authors can make their results available to the community, in citable form, before we publish the edited article. We will replace this *Accepted Manuscript* with the edited and formatted *Advance Article* as soon as it is available.

You can find more information about *Accepted Manuscripts* in the [Information for Authors](#).

Please note that technical editing may introduce minor changes to the text and/or graphics, which may alter content. The journal's standard [Terms & Conditions](#) and the [Ethical guidelines](#) still apply. In no event shall the Royal Society of Chemistry be held responsible for any errors or omissions in this *Accepted Manuscript* or any consequences arising from the use of any information it contains.

Cite this: DOI: 10.1039/c0xx00000x

www.rsc.org/xxxxxx

ARTICLE TYPE

# Luminescent properties of a new green afterglow phosphor NaBaScSi<sub>2</sub>O<sub>7</sub>:Eu<sup>2+</sup>

Gen Li, Yuhua Wang,\* Wei Zeng, Wenbo Chen, Shaochun Han, Haijie Guo and Xicheng Wang

Received (in XXX, XXX) Xth XXXXXXXXX 20XX, Accepted Xth XXXXXXXXX 20XX

DOI: 10.1039/b000000x

A novel green afterglow phosphor NaBaScSi<sub>2</sub>O<sub>7</sub>:Eu<sup>2+</sup> was prepared by a solid state reaction under a reductive atmosphere. The NaBaScSi<sub>2</sub>O<sub>7</sub>:Eu<sup>2+</sup> phosphor shows two emission bands centered at about 424 (weak) and 502 nm (strong) due to the substitution of Eu<sup>2+</sup> in both Ba<sup>+</sup> and Na<sup>2+</sup> sites, and energy transfer from Eu<sub>Ba</sub> (424 nm) to Eu<sub>Na</sub> (502 nm) was found. Both Eu<sub>Ba</sub> and Eu<sub>Na</sub> has contribution to the afterglow process while Eu<sub>Na</sub> dominates. Na<sub>0.99</sub>BaScSi<sub>2</sub>O<sub>7</sub>:0.01Eu<sup>2+</sup> exhibits green long lasting phosphorescence, whose duration is more than 1 h. The thermoluminescence property of NaBaScSi<sub>2</sub>O<sub>7</sub>:Eu<sup>2+</sup> and the relationship between thermoluminescence and thermal quenching property were discussed in detail. This work provides a new and efficient candidate for the long lasting phosphorescence material.

## 1. Introduction

Energy is one of the most focused topics in the 21st century. The development of science and technology brings about the increasing demand of energy sources. The unprecedented global increase in energy consumption has inevitably caused some problems. For example, due to the increasingly rapid exploit of conventional energy sources, such as the fossil fuels, the environmental pollution is more and more serious. As it is well known, solar energy is a renewable and clean energy source. Enhancing the ability of solar energy utilization should effectively alleviate these severe problems and ensure the sustainable development of our society and economy.<sup>1-4</sup> Therefore, there is a great requirement to develop a reliable storage and utilization technology of solar energy.

As a novel and efficient solar energy material, long lasting phosphorescence (LLP) material has attracted hectic researches in recent years. The materials relate to an interesting optical phenomenon that the luminescence still can be observed for several seconds to hours after the stoppage of excitation.<sup>5,6</sup> They can absorb and store energy under the excitation (such as sunlight and some other artificial light source) and then release the stored energy in the form of light at room temperature under thermal stimulation. Due to the environmentally friendly, energy saving and recyclable properties, LLP materials can be applied in extensive important fields, e.g. emergency signs, decorations, electronic displays, solar energy utilization, imaging or optical memory storage, medical diagnostics and *vivo* bio-imaging, etc.<sup>7-11</sup>

At present, the best LLP materials are still Eu<sup>2+</sup> doped alkaline earth aluminate phosphors, e.g. SrAl<sub>2</sub>O<sub>4</sub>:Eu<sup>2+</sup>, Dy<sup>3+</sup> (green) and CaAl<sub>2</sub>O<sub>4</sub>:Eu<sup>2+</sup>, Nd<sup>3+</sup> (blue).<sup>12-16</sup> However, the aluminate-based LLP materials have bad water resistance. Besides, the synthetic process usually needs H<sub>3</sub>BO<sub>3</sub> as a flux and the synthetic

temperature of these materials is usually too high (>1400 °C).<sup>12,13</sup> These disadvantages limit the practical application of LLP materials. Compared with aluminate-based LLP materials, the silicate-based LLP materials possess better chemical stability, heat stability, weather resistance and lower synthetic temperature so that they have attracted more and more attention recently.<sup>17-19</sup> Unfortunately, the excellent silicate-based LLP materials are still limit to Sr<sub>2</sub>MgSi<sub>2</sub>O<sub>7</sub>:Eu<sup>2+</sup>, Dy<sup>3+</sup> (blue)<sup>20</sup> and Ca<sub>2</sub>MgSi<sub>2</sub>O<sub>7</sub>:Eu<sup>2+</sup>, Dy<sup>3+</sup> (yellow-green)<sup>21</sup>, and their afterglow intensities are weaker than those excellent aluminate-based LLP materials. Therefore, the development of new silicate-based LLP materials would be necessary to meet the demand of practical utilization.

Generally, the design of LLP materials is based on the host and activator. In 2010, the silicate NaBaScSi<sub>2</sub>O<sub>7</sub> compound was first reported in the form of a single crystal, which has a monoclinic system with a space-group symmetry of P2<sub>1</sub>/m.<sup>22</sup> Later, the structure and luminescence properties of NaBaScSi<sub>2</sub>O<sub>7</sub>:Eu<sup>2+</sup> polycrystalline powder were studied in detail by Ray et al., Liu et al. and Zhu et al.<sup>23-25</sup> This phosphor with high luminescence efficiency attracts our intense interest and none of its LLP properties has been studied yet upon reviewing the literature. Additionally, until now it is well known that Eu<sup>2+</sup> acting as an efficient activator is a common ion widely investigated and applied in the field of LLP materials because its 5d electron state is usually close to the conduction band of the host, which makes trapping of electron become possible.<sup>26-28</sup> Accordingly, NaBaScSi<sub>2</sub>O<sub>7</sub>:Eu<sup>2+</sup> was selected as the silicate-based candidate in our work for the sake of basic scientific study and demand for LLP materials. Just as we anticipated, in this paper, a novel green emitting LLP material, NaBaScSi<sub>2</sub>O<sub>7</sub>:Eu<sup>2+</sup>, was successfully prepared by a solid state reaction under reductive atmosphere and identified by XRD refinement. The photoluminescence, afterglow and thermoluminescence properties of NaBaScSi<sub>2</sub>O<sub>7</sub>:Eu<sup>2+</sup>

phosphors were investigated in detail for the first time.

## 2. Experimental

### 2.1. Synthesis

Powder samples of  $\text{NaBa}_{1-x}\text{ScSi}_2\text{O}_7:x\text{Eu}^{2+}$  ( $0 \leq x \leq 0.025$ ) were synthesized by conventional solid state reaction method. The raw materials  $\text{Na}_2\text{CO}_3$  (99%),  $\text{BaCO}_3$  (99.9%),  $\text{SiO}_2$  (99.9%),  $\text{Sc}_2\text{O}_3$  (99.99%) and  $\text{Eu}_2\text{O}_3$  (99.99%) were stoichiometrically weighted out. After the ingredients were mixed thoroughly, the mixtures were placed into an alumina crucible and sintered at  $1250^\circ\text{C}$  for 5 h under a reductive atmosphere (5%  $\text{H}_2$  + 95%  $\text{N}_2$ ) in an electric tube furnace. Finally, after calcination, the samples were cooled to room temperature in the furnace and ground again into powder for subsequent use.

### 2.2. Characterization

The phase purity of samples was analyzed by X-ray powder diffraction (XRD) using a Bruker D2 PHASER X-ray diffractometer with graphite monochromator using  $\text{Cu K}\alpha$  radiation ( $\lambda = 1.54184 \text{ \AA}$ ), operating at 30 kV and 15 mA with a scanning step of  $0.02^\circ$  in the  $2\theta$  range from  $10^\circ$  to  $80^\circ$ . The morphology of the sample and the energy dispersive X-ray spectroscopy (EDS) spectrum were detected by field emission scanning electron microscopy (FESEM, Hitachi, S-4800). Photoluminescence emission (PL), excitation (PLE) and phosphorescence spectra were carried out by a FLS-920T spectrometer with Xe 900 (450 W xenon arc lamp) as the light source. The scanning step was 1 nm. Thermal quenching was tested using a heating apparatus (TAP-02) in combination with PL equipment. Afterglow decay curve measurements were measured with a PR305 long afterglow instrument after the samples were irradiated with standard artificial daylight (the color temperature 6500 K and the power 18 W) for 10 min. Thermoluminescence (TL) curves were measured with a FJ-427A TL meter (Beijing Nuclear Instrument Factory) with a heating rate of  $1 \text{ K s}^{-1}$ . The sample weight was kept constant (20 mg). Before the measurements, the samples were irradiated with ultraviolet light (254 nm) for 15 min. All the measurements were carried out at room temperature except for thermal quenching and TL curves. The results are repeatable.

## 3. Results and discussion

### 3.1. Phase analysis

Fig. 1a shows Rietveld structural refinement of the XRD pattern of  $\text{NaBaScSi}_2\text{O}_7$  host, obtained using Materials Studio program. Red solid line, black crosses and blue solid line are the calculated pattern, experimental pattern and background, respectively. Pink short vertical lines show the positions of Bragg reflections of the calculated pattern. The difference between experimental and calculated pattern is plotted by dark cyan line at the bottom. For the structure refinement, initial structural model is constructed with the single crystal data (COD-9013815).<sup>22</sup> The final refinement residual factors are  $R_{\text{wp}} = 8.52\%$  and  $R_p = 5.39\%$ . The refinement results confirm the single-phase nature of the compound in the monoclinic space group  $\text{P}2_1/\text{m}$  (No. 11) with cell parameters  $a = 6.86117 \pm 0.00133 \text{ \AA}$ ,  $b = 5.61656 \pm 0.00108 \text{ \AA}$  and  $c = 8.81239 \pm 0.00164 \text{ \AA}$ , which almost coincides with the

unit cell parameters of the reported  $\text{NaBaScSi}_2\text{O}_7$  host.<sup>22</sup> According to Zhu's report,  $\text{Eu}^{2+}$  occupies both the  $\text{Na}^+$  and  $\text{Ba}^{2+}$  sites in  $\text{NaBaScSi}_2\text{O}_7$ .<sup>25</sup> As shown in the inset of Fig. 1a, the  $\text{Ba}^{2+}$  site is coordinated with nine oxygen ions and the  $\text{Na}^+$  site is coordinated with eight oxygen ions. The ionic radii of  $\text{Na}^+$  and  $\text{Ba}^{2+}$  are 1.18 and 1.47  $\text{ \AA}$ , and the ionic radii for the eight- and nine-coordinated  $\text{Eu}^{2+}$  are 1.25 and 1.30  $\text{ \AA}$ , which shows that the difference in ionic radii between the doped and substituted ions is acceptable.<sup>29</sup> Divalent  $\text{Eu}^{2+}$  replaces the divalent  $\text{Ba}^{2+}$  site equivalently, while replaces the monovalent  $\text{Na}^+$  site with the charge imbalance, resulting in generation of vacancies. Fig. 1b shows the EDS spectrum analysis of the  $\text{NaBaScSi}_2\text{O}_7$  sample. It confirms the presence of sodium (Na), barium (Ba), scandium (Sc), silicon (Si), oxygen (O) and carbon (C) in the  $\text{NaBaScSi}_2\text{O}_7$  sample. Except for C, which is deduced from the use of conductive adhesive tape for supporting the sample, no other impurity peaks can be detected. The SEM image of  $\text{NaBaScSi}_2\text{O}_7$  host is shown in the inset of Fig. 1b. It is clearly seen that the grains have irregular shape of blocky particles with a size of about 2-20  $\mu\text{m}$ .

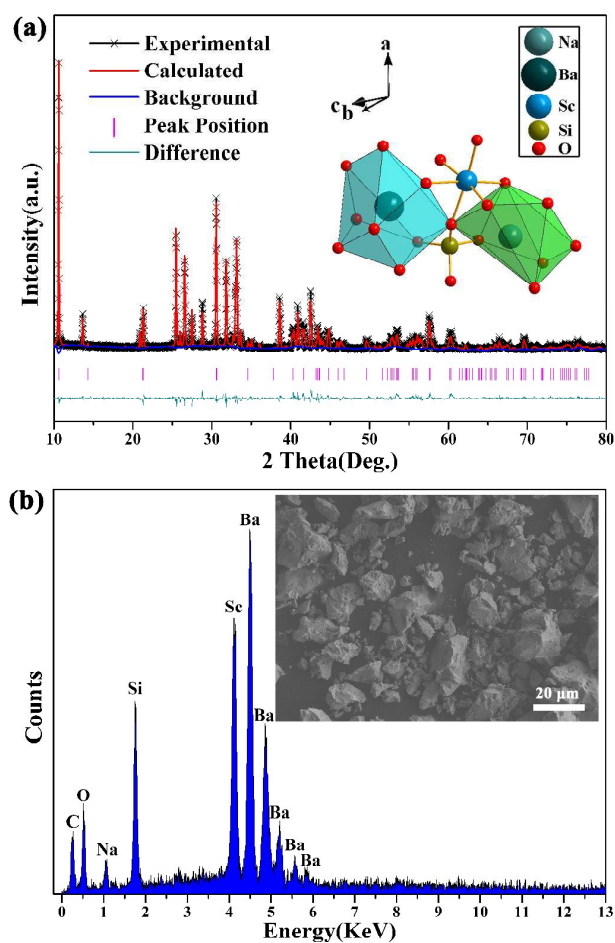


Fig. 1 (a) XRD refinement results of  $\text{NaBaScSi}_2\text{O}_7$  host. (b) the EDS spectrum of  $\text{NaBaScSi}_2\text{O}_7$  host. The inset shows SEM image of  $\text{NaBaScSi}_2\text{O}_7$  host.

Fig. 2 shows a series of XRD patterns for  $\text{NaBa}_{1-x}\text{ScSi}_2\text{O}_7:x\text{Eu}^{2+}$  ( $0 \leq x \leq 0.025$ ) phosphors with different  $\text{Eu}^{2+}$  concentrations as well as the calculated XRD patterns of  $\text{NaBaScSi}_2\text{O}_7$  host

according to the refinement results. It is obvious that the XRD profiles are well fitted with the calculated XRD pattern and diffraction peaks of these phosphors can be exactly assigned to NaBaScSi<sub>2</sub>O<sub>7</sub> host. No detectable impurity phase is observed in the obtained phosphors, indicating that all the samples are single phase and Eu<sup>2+</sup> has been successfully incorporated in the NaBaScSi<sub>2</sub>O<sub>7</sub> host without changing the crystal structure noticeably.

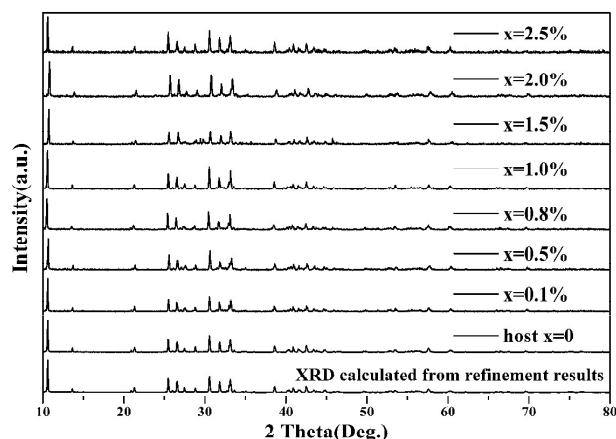


Fig. 2 XRD patterns of NaBa<sub>1-x</sub>ScSi<sub>2</sub>O<sub>7</sub>:xEu<sup>2+</sup> (0 ≤ x ≤ 0.025) and the calculated XRD pattern from the refinement results.

### 3.2. Photoluminescence analysis

In order to investigate the luminescence properties, a series of samples with different Eu<sup>2+</sup> concentration, Na<sub>1-x</sub>BaScSi<sub>2</sub>O<sub>7</sub>:xEu<sup>2+</sup> (0.001 ≤ x ≤ 0.025), were synthesized. Fig. 3a illustrates the PLE and PL spectra of the Eu<sup>2+</sup> doped NaBaScSi<sub>2</sub>O<sub>7</sub> phosphor. Under 368 nm excitation, the PL spectra of the NaBaScSi<sub>2</sub>O<sub>7</sub>:Eu<sup>2+</sup> phosphors consist of two emission bands centered at about 424 and 502 nm, which is consistent with the result of Zhu's report<sup>25</sup>. In that report, the conclusion was drawn that the former emission band centered at 424 nm is attributed to the 5d-4f transitions of Eu<sup>2+</sup> occupying Ba<sup>2+</sup> sites with nine-coordination (Eu<sub>Ba</sub>), and the latter emission band centered at 502 nm is attributed to the 5d-4f transitions of Eu<sup>2+</sup> occupying the Na<sup>+</sup> site with eight-coordination (Eu<sub>Na</sub>), respectively. The intensity of the latter emission band centered at 502 nm is strong while that of the former one centered at 424 nm is weak, which results in a green emission of the NaBaScSi<sub>2</sub>O<sub>7</sub>:Eu<sup>2+</sup> phosphor. The PLE spectra of Na<sub>0.99</sub>BaScSi<sub>2</sub>O<sub>7</sub>:0.01Eu<sup>2+</sup> are monitored at 424 and 502 nm. Both the obtained broad bands are assigned to the transition between the ground-state 4f<sup>7</sup> and the crystal-field split 4f<sup>6</sup>5d<sup>1</sup> configuration of Eu<sup>2+</sup>.<sup>30</sup> When monitored at 424 nm (Eu<sub>Ba</sub>), the PLE spectrum exhibits a broad excitation band from 250 to 380 nm, which could be mainly originated from the absorption of Eu<sub>Ba</sub>. When the monitoring wavelength is fixed at 502 nm (Eu<sub>Na</sub>), the PLE spectrum shows a wider excitation band from 250 to 500 nm. The additional excitation band from 380 to 500 nm should be mainly ascribed to the absorption of Eu<sub>Na</sub>. Both Eu<sub>Na</sub> and Eu<sub>Ba</sub> are found, indicating that Eu<sub>Na</sub> is essentially excited through Eu<sub>Ba</sub>, which provides an evidence for the energy transfer (ET) between Eu<sub>Ba</sub> and Eu<sub>Na</sub> in NaBaScSi<sub>2</sub>O<sub>7</sub>.

Fig. 3b represents the dependence of the emission intensity at 424 nm and the emission intensity at 502 nm on Eu<sup>2+</sup> concentration

for Na<sub>1-x</sub>BaScSi<sub>2</sub>O<sub>7</sub>:xEu<sup>2+</sup> samples, respectively. The emission intensity at 502 nm increases with an increase of the Eu<sup>2+</sup> doping concentration. And it reaches a maximum value at the 1% Eu<sup>2+</sup> concentration. Since the Eu<sup>2+</sup> concentration surpasses 1%, the emission intensity illustrates a decrease tendency due to the concentration quenching effect. That is, when the Eu<sup>2+</sup> concentration increases, more and more Eu<sup>2+</sup> pair or aggregate with others. Efficient resonant energy transfer between Eu<sup>2+</sup> ions and a fraction of migration to distant luminescent killer occur, leading to the luminescence quenching. It is interesting that, comparatively, the emission intensity at 424 nm changes in different way with an increase of the Eu<sup>2+</sup> concentration. It decreases firstly and then increases, finally reaches a saturation point at x = 0.02.

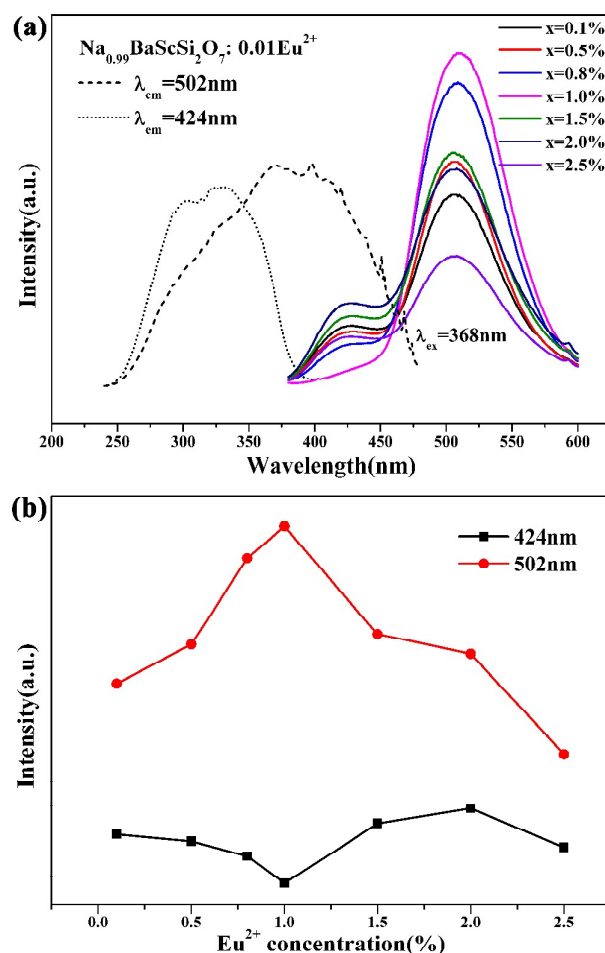


Fig. 3 (a) PLE and PL spectra of Na<sub>1-x</sub>BaScSi<sub>2</sub>O<sub>7</sub>:xEu<sup>2+</sup> (0.001 ≤ x ≤ 0.025). (b) The dependence of the emission intensity at 424 nm (black) and 502 nm (red) on Eu<sup>2+</sup> ion concentration for Na<sub>1-x</sub>BaScSi<sub>2</sub>O<sub>7</sub>:xEu<sup>2+</sup> samples, respectively.

Generally, ET occurs only when the emission band of the sensitizer overlaps spectrally with the absorption band of the activator.<sup>31</sup> Spectral overlap has been observed in Eu<sub>Ba</sub> emission and Eu<sub>Na</sub> excitation in NaBaScSi<sub>2</sub>O<sub>7</sub>, which is shown in Fig. 3a. It can be seen that the overlap of Eu<sub>Ba</sub> emission and Eu<sub>Na</sub> excitation is almost 100%, which indicates that the ET from Eu<sub>Ba</sub> to Eu<sub>Na</sub> is possible. Thus, it should be believed that, in Na<sub>1-x</sub>BaScSi<sub>2</sub>O<sub>7</sub>:xEu<sup>2+</sup>, energy can transfer in three ways: Eu<sub>Ba</sub>-Eu<sub>Ba</sub>,

$\text{Eu}_{\text{Ba}}-\text{Eu}_{\text{Na}}$  and  $\text{Eu}_{\text{Na}}-\text{Eu}_{\text{Na}}$ .

Since  $\text{Eu}^{2+}$  is very sensitive to its crystal environment, as a consequence,  $\text{Eu}^{2+}$  located at the different crystallographic sites in host lattices exhibit different emission bands.<sup>32</sup> In  $\text{NaBaScSi}_2\text{O}_7:\text{Eu}^{2+}$ , the two kinds of emitting centers at 424 and 502 nm have been labeled as  $\text{Eu}_{\text{Ba}}$  and  $\text{Eu}_{\text{Na}}$  respectively, and the ET between them can be expected. When the concentration of  $\text{Eu}^{2+}$  is relative low, the distance between vicinal  $\text{Eu}_{\text{Ba}}$  ions is too large while the distance between  $\text{Eu}_{\text{Ba}}$  and  $\text{Eu}_{\text{Na}}$  ions is near relatively so that ET from  $\text{Eu}_{\text{Ba}}$  to  $\text{Eu}_{\text{Na}}$  is dominant, and the probability of ET from  $\text{Eu}_{\text{Ba}}$  to  $\text{Eu}_{\text{Na}}$  increases as the distance between  $\text{Eu}_{\text{Ba}}$  and  $\text{Eu}_{\text{Na}}$  ions decreases, resulting in that the  $\text{Eu}_{\text{Ba}}$  emission intensity decreases firstly with increasing  $\text{Eu}^{2+}$  concentration. As the  $\text{Eu}^{2+}$  concentration increases to 1%, the distance between vicinal  $\text{Eu}_{\text{Ba}}$  ions becomes less, thus resulting in that ET from one  $\text{Eu}_{\text{Ba}}$  ion to another is dominant. In this circumstances, the  $\text{Eu}_{\text{Ba}}$  emission intensity increases with the increase of the  $\text{Eu}^{2+}$  concentration. However, as the  $\text{Eu}^{2+}$  concentration increases continually and surpasses 2%, the concentration quenching effect occurs so that the  $\text{Eu}_{\text{Ba}}$  emission intensity illustrates a decrease tendency finally.

### 3.3. Afterglow characteristic

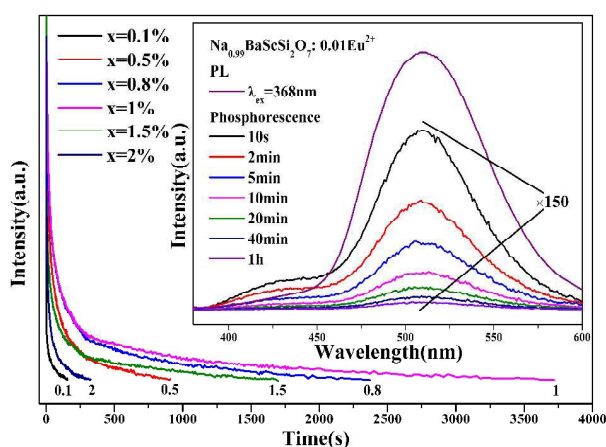


Fig. 4 The afterglow decay curves of  $\text{Na}_{1-x}\text{BaScSi}_2\text{O}_7:x\text{Eu}^{2+}$  ( $0.001 \leq x \leq 0.02$ ). The inset shows the PL spectrum and phosphorescence spectra of  $\text{Na}_{0.99}\text{BaScSi}_2\text{O}_7:0.01\text{Eu}^{2+}$ .

Fig. 4 depicts the afterglow decay curves of  $\text{Na}_{1-x}\text{BaScSi}_2\text{O}_7:x\text{Eu}^{2+}$  ( $0.001 \leq x \leq 0.02$ ) with different  $\text{Eu}^{2+}$  concentrations. The optimal  $\text{Eu}^{2+}$  concentration for the longest afterglow time of  $\text{NaBaScSi}_2\text{O}_7:\text{Eu}^{2+}$  is 1%. The persistent emission lasts for more than 1 h.

The inset of Fig. 4 shows the PL spectrum of  $\text{Na}_{0.99}\text{BaScSi}_2\text{O}_7:0.01\text{Eu}^{2+}$  under 368 nm excitation and its phosphorescence spectra measured at different time after the excitation source was switched off. The phosphorescence spectra are plotted with an amplification of 150 times. They also reveal two broad bands and their profiles do not change with decay time, indicating that the green LLP originates from the two kinds of  $\text{Eu}^{2+}$  emission centers. From the phosphorescence spectra, it is safe to say that the phosphorescence should be derived from  $\text{Eu}^{2+}$  in the above-mentioned  $\text{Ba}^{2+}$  and  $\text{Na}^+$  site and the  $\text{Eu}_{\text{Na}}$  emission should be dominant apparently.

### 3.4. Thermoluminescence characteristic

It is well known that energy traps play an essential role for photoenergy storage in LLP materials, which have great effect on the afterglow performance.<sup>33</sup> In general, TL technique is a very useful tool to obtain the information with regard to the energy trap depth and density.<sup>34</sup> With different  $\text{Eu}^{2+}$  concentration, all TL curves show four TL peaks at the same positions approximately, corresponding to 87 ( $T_1$ ), 130 ( $T_2$ ), 229 ( $T_3$ ) and 365 °C ( $T_4$ ), respectively. There is no variation of their profiles except for their intensities, so the TL curve of the  $\text{Na}_{0.99}\text{BaScSi}_2\text{O}_7:0.01\text{Eu}^{2+}$  sample is exhibited merely in Fig. 5.

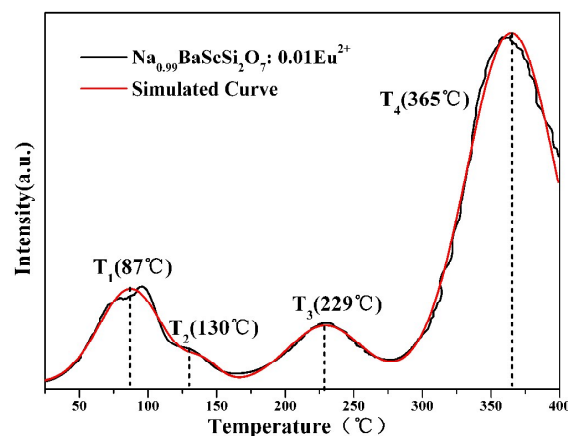


Fig. 5 TL curve of  $\text{Na}_{0.99}\text{BaScSi}_2\text{O}_7:0.01\text{Eu}^{2+}$ .

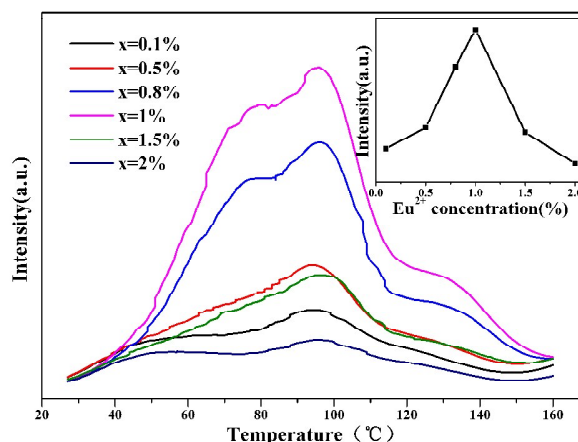


Fig. 6 TL curves of  $\text{Na}_{1-x}\text{BaScSi}_2\text{O}_7:x\text{Eu}^{2+}$  ( $0.001 \leq x \leq 0.02$ ). The inset shows the dependence of the  $T_1$  intensity on  $\text{Eu}^{2+}$  concentration for  $\text{Na}_{1-x}\text{BaScSi}_2\text{O}_7:x\text{Eu}^{2+}$  samples.

It is well known that the TL peak at somewhere between 50 and 150 °C is suitable for LLP materials to free the trapped carriers slowly by thermal energy at room temperature.<sup>35,36</sup> So neither  $T_3$  nor  $T_4$  is appropriate for creating afterglow phenomenon.  $T_1$  and  $T_2$  are exactly the traps which lead to the afterglow phenomenon in the  $\text{Na}_{1-x}\text{BaScSi}_2\text{O}_7:x\text{Eu}^{2+}$  phosphors and  $T_1$  is dominant. In order to investigate the relationship between TL characteristic and afterglow characteristic, the TL curves from 25 to 160 °C of  $\text{Na}_{1-x}\text{BaScSi}_2\text{O}_7:x\text{Eu}^{2+}$  ( $0.001 \leq x \leq 0.02$ ) samples are given in Fig. 6, and the inset shows the dependence of the  $T_1$  intensity on  $\text{Eu}^{2+}$  concentration. It is found that, with increasing the  $\text{Eu}^{2+}$  concentration,  $T_1$  and  $T_2$  increase at first and decreases when the concentration is beyond 1%, which corresponds to the variation tendency of the afterglow decay time. Due to the nonequivalent

substitution, an excess of positive charge in the host must be compensated. The only possible way to fulfill the charge compensation is that one  $\text{Eu}^{2+}$  replace two  $\text{Na}^+$  to balance the charge of the phosphor, which results in large generation of defects,  $V_{\text{Na}}$ , as energy trap centers for photoenergy storage. As a consequence, with increasing the  $\text{Eu}^{2+}$  concentration, the number of energy trap centers should rise. And more and more excited electrons would be captured by traps rather than return immediately to emission centers, which is beneficial to the afterglow performance. However, as the distances of traps to traps or traps to emission centers decrease due to the increasing concentration, the excited electrons prefer to transfer from one center to another with non-radiative transition<sup>31,37,38</sup>, such as thermal energy, leading to the decrease of the direct radiation transition for afterglow, which corresponds to the variation tendency of the afterglow decay time.

### 3.5. Relationship between Thermoluminescence and Thermal quenching property

According to the previous reports, the  $\text{NaBaScSi}_2\text{O}_7:\text{Eu}^{2+}$  phosphor possesses an excellent thermal stability, even at high temperature.<sup>24,25</sup> In the thermoluminescence characteristic analysis discussed above, there are four TL peaks, corresponding to 87 ( $T_1$ ), 130 ( $T_2$ ), 229 ( $T_3$ ) and 365°C ( $T_4$ ) respectively, in the  $\text{NaBaScSi}_2\text{O}_7:\text{Eu}^{2+}$  phosphor. At room temperature, only  $T_1$  and  $T_2$  could free the trapped carriers to generate the afterglow while deep  $T_3$  and  $T_4$  could not. However, in the thermal quenching property investigation, deep  $T_3$  and  $T_4$  could free readily the trapped carriers to generate luminescence when measured the PL spectra at high temperature (eg. 200 or 250°C). Therefore, there is doubt that the thermoluminescence from the deep traps may play a role as compensation for the PL intensity and have a positive influence on the thermal quenching property of  $\text{NaBaScSi}_2\text{O}_7:\text{Eu}^{2+}$ .

For the sake of clarifying the relationship between the thermoluminescence and thermal quenching property of  $\text{NaBaScSi}_2\text{O}_7:\text{Eu}^{2+}$ , the following experimental procedures were performed. Before the thermal quenching test, the phosphor was heated at 500°C for 10 min to erase any residual trapped carriers. The  $\text{Na}_{0.99}\text{BaScSi}_2\text{O}_7:0.01\text{Eu}^{2+}$  phosphor without heat treatment is labeled as S1 while it is labeled as S2 with heat treatment at 500°C. As shown in Fig. 7a, the TL curves of S1 (black) and S2 (red) indicates apparently that the residual trapped carriers are erased after heat treatment in the S2 sample.

The temperature dependent emission spectra for S1 and S2 excited at 368 nm were measured and are illustrated in Fig. 7b, respectively. It can be seen obviously that all the emission intensities of S1 at different temperature are much stronger than that of S2. This phenomenon can be explained as follows. Generally, the excited electrons could directly return to the ground state and emit photons simultaneously. In the S2 sample, the residual trapped carriers have been erased through heat treatment. When irradiated by the excitation light source, the part excited electrons would be captured by the empty traps rather than return immediately to emission centers, resulting in the weak emission intensity.

As shown in the inset of Fig. 7b, the thermal quenching property of the commercial green phosphor (com-green LMS520B) have also been measured for comparison. As the same as previous

reports, the thermal stabilities of both S1 and S2 are found to be much better than that of the com-green phosphor LMS520B in this work. Surprisingly, S2 shows nearly the same thermal stability as S1. The unexpected result of the thermal stability comparison between S1 and S2 indicates that the excellent thermal stability of  $\text{NaBaScSi}_2\text{O}_7:\text{Eu}^{2+}$  is irrelevant to the TL. The traps in the  $\text{NaBaScSi}_2\text{O}_7:\text{Eu}^{2+}$  could influence the emission intensity while have little effect on the thermal quenching property. The excellent thermal stability should be an intrinsic property of the  $\text{NaBaScSi}_2\text{O}_7:\text{Eu}^{2+}$  phosphor, related to the crystal structure, valence band, chemical composition of the host lattice and doping concentration of the activator.<sup>39</sup>

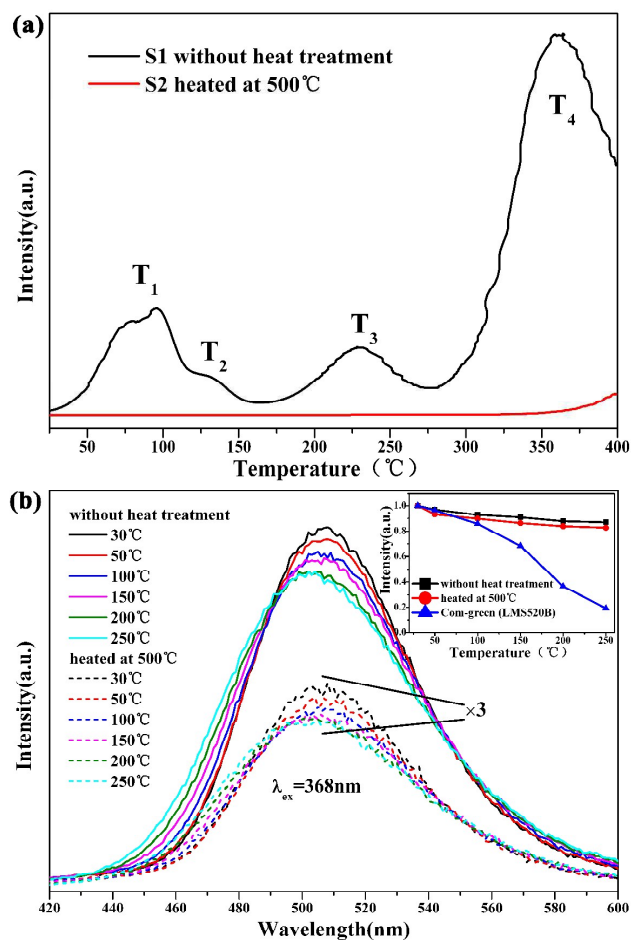


Fig. 7 (a) TL curves of S1 and S2. (b) The temperature dependent PL spectra of S1 and S2, the inset shows the thermal stabilities of S1 (solid), S2 (dot) and the com-green phosphor (LMS520B).

## 4. Conclusions

In summary, a novel green afterglow phosphor  $\text{NaBaScSi}_2\text{O}_7:\text{Eu}^{2+}$  is successfully synthesized by a solid state reaction. The PL spectra of the  $\text{NaBaScSi}_2\text{O}_7:\text{Eu}^{2+}$  phosphors consist of two emission bands centered at about 424 (weak) and 502 nm (strong), attributed to the 5d-4f transitions of  $\text{Eu}_{\text{Ba}}$  and  $\text{Eu}_{\text{Na}}$ , respectively. Energy transfer from  $\text{Eu}_{\text{Ba}}$  to  $\text{Eu}_{\text{Na}}$  is found. The green persistent emission of  $\text{NaBaScSi}_2\text{O}_7:\text{Eu}^{2+}$  can last for more than 1 h. It should be believed that  $T_1$  (87°C) and  $T_2$  (130°C) at the appropriate depth are exactly the traps which lead to the afterglow phenomenon in the  $\text{NaBaScSi}_2\text{O}_7:\text{Eu}^{2+}$  phosphors. The

experimental result indicates that the excellent thermal stability of NaBaScSi<sub>2</sub>O<sub>7</sub>:Eu<sup>2+</sup> is irrelevant to the TL.

## Acknowledgments

This work is supported by Specialized Research Fund for the Doctoral Program of Higher Education (Grant No.20120211130003) and the National Natural Science Funds of China (Grant No.51372105). Thanks for the support of Gansu Province Development and Reform Commission.

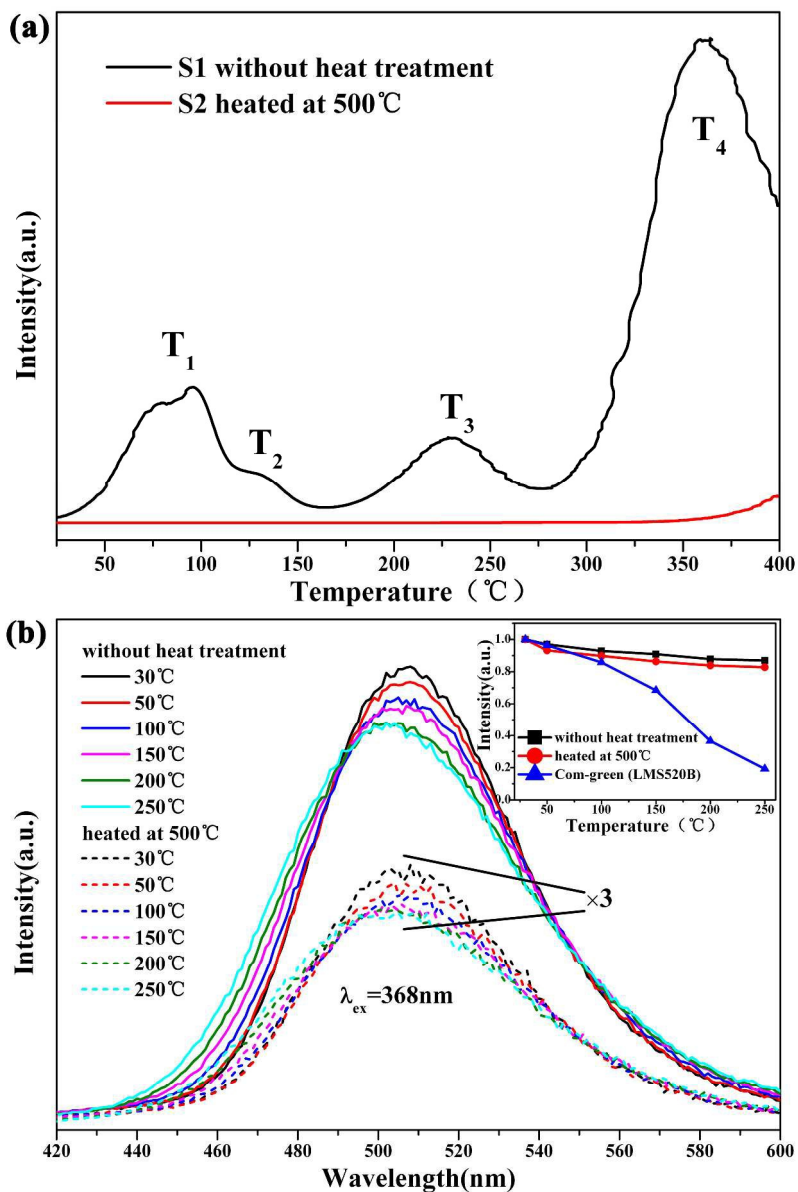
## Notes and references

<sup>10</sup> Department of Materials Science, School of Physical Science and Technology, Lanzhou University, Lanzhou, 730000, PR China and Key Laboratory for Special Function Materials and Structural Design of the Ministry of Education, Lanzhou University, Lanzhou 730000, China.

\*Corresponding author: Yuhua Wang

<sup>15</sup> Email address: wyh@lzu.edu.cn; tel.: +86 931 8912772; fax: +86 931 8913554.

1. P.F. Ribeiro, B.K. Johnson, M.L. Crow, A. Arsoy, Y. Liu, Proc. IEEE, 2001, 89, 1744-1756.
2. S.G. Chalk, J.F. Miller, J. Power Sources, 2006, 159, 73-80.
- <sup>20</sup> 3. Y.H. Jin, Y.H. Hu, L. Chen, Y.R. Fu, Z.F. Mu, T. Wang, J. Lin, J. Alloys Comp., 2014, 616, 159-165.
4. I. Hadjipaschalis, A. Poullikkas, V. Efthimiou, Renew. Sust. Energy Rev., 2009, 13, 1513-1522.
5. Z. Pan, Y. Y. Lu and F. Liu, Nat. Mater., 2012, 11, 58-63.
- <sup>25</sup> 6. X. Yu, X. Xu, H. Yu, T. Jiang, P. Yang, Q. Jiao and J. Qiu, Mater. Res. Bull., 2012, 47, 2696-2699.
7. A. Bessière, Suchinder K. Sharma, N. Basavaraju, K.R. Priolkar, L. Binet, B. Viana, A.J.J. Bos, T. Maldiney, C. Richard, D. Scherman, D. Gourier, Chem. Mater., 2014, 26, 1365-1373.
- <sup>30</sup> 8. L.L. Noto, M.L. Chithambo, O.M. Ntwaeaborwa, H.C. Swart, J. Alloys Comp., 2014, 589, 88-93.
9. H. A. Hoppe, H. Lutz, P. Morys, W. Schnick and A. Seilmeier, J. Phys. Chem. Solids, 2000, 61, 2001-2006.
10. M. Kowatari, D. Koyama, Y. Satoh, K. Iinuma and S. Uchida, Nucl. Instrum. Methods Phys. Res., Sect. A, 2002, 480, 431-439.
- <sup>35</sup> 11. C. N. Xu, T. Watanabe, M. Akiyama and X. G. Zheng, Appl. Phys. Lett., 1999, 74, 2414-2416.
12. T. Matsuzawa, Y. Aoki, N. Takeuchi, and Y. Murayama, J. Electrochem. Soc., 1996, 143, 2670-2673.
- <sup>40</sup> 13. Y. Gong, Y.H. Wang, Y.Q. Li, X.H. Xu, and W. Zeng, Opt. Express, 2011, 19, 4310-4315.
14. D.S. Kshatri, A. Khare, J. Alloys Comp., 2014, 585, 488-495.
15. W. Xie, J. Quan, H.Y. Wu, L.X. Shao, C.W. Zou, J. Zhang, X.Y. Shi, Y.H. Wang, J. Alloys Comp., 2012, 514, 97-102.
- <sup>45</sup> 16. T. Katsumata, H. Kubo, S. Komuro, H. Aizawa, J. Am. Ceram. Soc., 2014, 97, 1704-1707.
17. T. L. Barry, J. Electrochem. Soc., 1968, 115, 1181-1183.
18. Y. Lin, Z. Tang, Z. Zhang, X. Wang, and J. Zhang, J. Mater. Sci. Lett., 2001, 20, 1505-1506.
- <sup>50</sup> 19. Y. Lin, Z. Zhang, Z. Tang, X. Wang, and Z. Zheng, J. Eur. Ceram. Soc., 2001, 21, 683-685.
20. C. Shi, Y. Fu, B. Liu, G. Zhang, Y. Chen, Z. Qi, and X. Luo, J. Lumin., 2007, 122-123, 11-13.
21. L. Jiang, C. Chang, D. Mao, and C. Feng, Opt. Mater., 2004, 27, 51-55.
- <sup>55</sup> 22. W. W. Maria, K. Uwe and T. Ekkehart, Can. Mineral., 2010, 48, 51-68.
23. S. Ray, K. Toda, S. Kamei, T. Ishigaki, K. Uematsu, M. Sato, H. Kato, M. Kobayashi and M. Kakihana, The 12<sup>th</sup> International Meeting on Information Display, Daegu, Korea, 2012, 42.
- <sup>60</sup> 24. C.Y. Liu, Z.G. Xia, Z.P. Lian, J. Zhou and Q.F. Yan, J. Mater. Chem. C, 2013, 1, 7139-7147.
25. G. Zhu, Y.R. Shi, M. Mikami, Y. Shimomura and Y.H. Wang, CrystEngComm, 2014, 16, 6089-6097.
- <sup>65</sup> 26. D. Jia, W. Jia, D. Evans, W. Dennis, H. Liu, J. Zhu, and W. Yen, J. Appl. Phys., 2000, 88, 3402-3407.
27. Y.Q. Li, Y.H. Wang, Y. Gong, X.H. Xu and M.J. Zhou, Opt. Express, 2010, 18, 24853-24858.
28. F. Clabau, X. Rocquefelte, T. Le Mercier, P. Deniard, S. Jobic, and M. Whangbo, Chem. Mater., 2006, 18, 3212-3220.
- <sup>70</sup> 29. R. D. Shannon, Acta Crystallogr., 1976, 32, 751-767.
30. G. Blasse and B. C. Grabmaier, Luminescent Materials, Springer-Verlag, Berlin, 1994.
31. D.L. Dexter, J. Chem. Phys., 1953, 21, 836-850.
- <sup>75</sup> 32. X. Yu, X.H. Xu, H.L. Yu, T.M. Jiang, P.H. Yang, Q. Jiao, J.B. Qiu, Mater. Res. Bull., 2012, 47, 2696-2699.
33. D. Jia, W. Jia, D. R. Evans, W. M. Dennis, H. Liu, J. Zhu and W. M. Yen, J. Appl. Phys., 2000, 88, 3402-3407.
34. J. Glodo and A. Wojtowicz, J. Alloys Compd., 2000, 300, 289-294.
- <sup>80</sup> 35. T. Aitasalo, P. Deren, J. Holsa, H. Junger, J. C. Krupa, M. Lastusaari, J. Legendziewicz, J. Niittykoski and W. Strek, J. Solid State Chem., 2003, 171, 114-122.
36. T. Kinoshita, M. Yamazaki, H. Kawazoe and H. Hosono, J. Appl. Phys., 1999, 86, 3729-3733.
- <sup>85</sup> 37. H. Yu, D.G. Deng, S.Q. Xu, C.P. Yu, H.Y. Yin, Q.L. Nie, J. Lumin., 2012, 132, 2553-2556.
38. G. Li, Y.H. Wang, W. Zeng, S.C. Han, W.B. Chen, Y.Y. Li, H. Li, Opt. Mater., 2014, 36, 1808-1813.
39. C.N. Zhang, T. Uchikoshi, R.J. Xie, L.H. Liu, Y.J. Cho, Y. Sakka, N. Hirosaki and T. Sekiguchi, J. Mater. Chem. C, 2015, DOI: 10.1039/c5tc01575h.



(a) TL curves of S1 and S2. (b) The temperature dependent PL spectra of S1 and S2, the inset shows the thermal stabilities of S1 (solid), S2 (dot) and the com-green phosphor (LMS520B).  
323x480mm (300 x 300 DPI)